Baniasadi, Hossein; Seppälä, Jukka; Kankkunen, Ari; Seppälä, Ari; Yazdani, Roza

Water-resistant gum-based phase change composite for thermo-regulating insulation packaging

Published in:
Journal of Energy Storage

DOI:
10.1016/j.est.2023.106725

Published: 01/05/2023

Document Version
Publisher's PDF, also known as Version of record

Please cite the original version:
Baniasadi, H., Seppälä, J., Kankkunen, A., Seppälä, A., & Yazdani, R. (2023). Water-resistant gum-based phase change composite for thermo-regulating insulation packaging. *Journal of Energy Storage*, *61*, Article 106725. https://doi.org/10.1016/j.est.2023.106725

Journal of Energy Storage 61 (2023) 106725

Contents lists available at ScienceDirect

Journal of Energy Storage

journal homepage: www.elsevier.com/locate/est

Research Papers

Water-resistant gum-based phase change composite for thermo-regulating insulation packaging

Hossein Baniasadi [a], Jukka Seppälä [a], Ari Kankkunen [b], Ari Seppälä [b], Maryam Roza Yazdani [b,*]

[a] Polymer Technology, School of Chemical Engineering, Aalto University, Espoo, Finland
[b] Department of Mechanical Engineering, School of Engineering, Aalto University, P.O. Box 14400, 00076 Aalto, Finland

ARTICLE INFO

Keywords:
Phase change materials
Gum Tragacanth biopolymer
Insulation
Water resistance
Thermal energy storage

ABSTRACT

The world's current energy crisis calls for green energy solutions that can preserve energy while incorporating renewable. As such, we have developed a leakage-proof phase change material (PCM) embedded in a biopolymeric matrix as a lightweight yet strong bio-based phase change composite (PCC) for passive energy storage and insulation purposes in packaging. This bio-based composite consists of gum tragacanth (GT) biopolymer and polyethylene glycol (PEG) PCM. It is further incorporated with biochar (BC) or mineral additive, i.e., Cloisite Na^+, to enhance its mechanical strength and thermal stability, which are among the main challenges for insulation materials. A hydrophobic layer of octadecyl isocyanate (ODI) is developed on the surface of the composite to increase its water resistance. The composite provides a hydrophobic surface with a minor water uptake capacity of 3.6 ± 0.3 % after one-week immersion in the water. It shows high latent heat storage up to 160 J g^{-1} and a stable phase change behavior, as demonstrated by over 100 differential scanning calorimetry heating-cooling cycles. It also possesses notable compressive mechanical properties, which were improved significantly after incorporating BC and Cloisite Na^+. The thermal conductivity of the composite is as low as 0.035 W m^{-1} K^{-1} manifesting in better thermal regulation compared with commercial polyethylene foams. This energy-positive bio-based solution combines the advantages of excellent insulation as a highly porous, lightweight, and strong composite with the latent heat and thermal inertia of PCM, making it suitable for transportation packaging of temperature-sensitive products.

1. Introduction

Heat flows as a result of a temperature difference between materials, while thermal insulation can inhibit the heat transfer between the materials where needed. Insulation materials are widely used in various areas of daily life, including electronics, buildings, packaging, transportation, etc. For example, by preventing hot or cold air from reaching inside, insulation reduces energy consumption in buildings or preserves products' quality in the transportation and packaging sectors. Proper transportation and storage of temperature-sensitive products such as food or medicine throughout the distribution process are essential for preserving product safety and quality. Temperature is one of the most critical factors for maintaining the quality of such products. Temperature fluctuations can reduce the quality, shorten shelf-life, and spoil perishables in the package during storage and/or transportation because the temperature can activate and accelerate undesired chemical reactions and microorganisms' growth. Thus, proper thermal insulation shipping/storage boxes are needed as they can protect the packed goods from thermal shocks and heat exchange with the environment and their consequent negative outcomes. Paperboard and polystyrene foam, as the most common traditional commercial packages, are ineffective against thermal fluctuations in transportation packaging due to their narrow thermal insulation as well as poor thermal buffering capacity [1–4]. Hence, new solutions, including packaging materials that can effectively minimize the impact of temperature fluctuations along the product supply/delivery chain, are of great interest. As such, the packaging should be organized to keep the product temperature within desired limits, thereby ensuring the products' safety, quality, and shelf-life.

Phase change materials (PCMs), also known as latent heat storage materials, can absorb and release a considerable amount of energy as latent heat of phase change by changing from solid to liquid phase and vice versa within a narrow temperature range [5,6]. PCMs can be incorporated with an insulation module to develop a passive temperature control performance package. The designed PCM-based insulations

---

* Corresponding author.
E-mail address: roza.yazdani@aalto.fi (M.R. Yazdani).

https://doi.org/10.1016/j.est.2023.106725
Received 18 October 2022; Received in revised form 5 January 2023; Accepted 17 January 2023

can then be employed during the transport, storage, and distribution stages of, for example, canned food, beverages, electronic circuits, as well as pharmaceutical and biomedical products to ensure that the products are in a relatively stable temperature environment [7–9]. PCMs can be classified as inorganics, such as salts and salt hydrates, or organic, like paraffin, fatty acids, and polyethylene glycol (PEG). Among these many PCMs, PEG has attracted wide interest in different fields, from electronic devices and solar thermal systems to automobiles and insulations, due to their favorable intrinsic characteristics such as biocompatibility, nontoxicity, non-corrosiveness as well as affordable large-scale cost perspective [10,11]. Besides, its melting point and enthalpy of fusion can range from 4 to 70 °C and 117–174 J g^{-1}, respectively, depending on its molecular weight. Nevertheless, like many other solid-to-liquid PCMs, PEG suffers from leakage issues during thermal energy storage, a large volume change during phase transitions, and low thermal stability, challenging their practical applications.

An effective way to overcome the drawbacks of PEG is embedding it into supporting matrices, e.g., a porous material carrier. With this solution, when the temperature reaches the phase change temperature of the in-housed PCM, i.e., PEG, it undergoes melting accompanied by a solid-to-liquid physical transition. At the same time, the supporting matrix preserves the PEG in its solid frame [10–12]. Accordingly, PEG has been trapped in the pores of porous materials upon capillary force and surface tension to create superior thermal storage materials with excellent stability [13–15].

On the other hand, due to the environmental impacts and large carbon footprints of conventional insulation materials, such as expanded polystyrene and polyurethane foams, renewable and bio-based materials with high porosity, low thermal conductivity, and high thermal stability have become of great interest for both academic research and practical applications. In this regard, plant-based materials, e.g., hemp, expanded cork, straw, grass, cellulose, etc., could be considered excellent candidates as thermal insulation materials thanks to their porous structure, a lower embodied energy than synthetic materials, and low thermal conductivity (0.037 and 0.080 W m^{-1} K^{-1}). Besides, they can be sourced locally [16–19]. Nevertheless, due to their hydrophilic nature, they suffer from poor water resistance, limiting their application as insulation materials. Thus, improving the weathering resistance is crucial for their practical engineering application. Accordingly, actions are needed to improve such materials' water resistance while maintaining their other relevant properties, such as low bulk density and high porosity. Hydrophobic coating is an efficient method for changing the surface from hydrophilic to hydrophobic without significantly impacting the other properties [20–22].

In this paper, we develop a gum tragacanth-based phase change composite (PCC) with leakage-free thermal regulation properties. To the best of our knowledge, gum tragacanth (GT) has neither been used to stabilize PCMs nor for insulation applications. As a plant-based material, GT is the dried exudates collected from the stems and branches of different species of *Astragalus*. GT is a heterogeneous and highly branched anionic polysaccharide consisting of water-soluble and water-swellable fragments. The soluble fraction, known as spheroidal, is a mixture of tragacanthic acid and arabinogalactan, while the swellable fraction, bassorin, is a complex of D-galacturonic acid methyl ester units. Fig. S1 shows the chemical structure of GT. Bassorin, constituting a major part of GT, has a high molecular weight ($M_w \sim 10^5$ Da) and an elongated (rodlike) molecular shape that provides a thick and heavy paste [23–25]. We hypothesized that GT could act as an excellent stabilizer for polar PEG in its melt state due to its molecular structure and hydrophilic characteristics enabled by the numerous hydrophilic functional groups such as hydroxyl and carboxyl. As such, several compositions of PCC insulation material are prepared via simple aqueous-based blending and adjusting the GT and PCM dry mass ratios to balance latent heat storage and insulation properties of the final product. The water resistance of the developed composite is then improved by coating a thin layer of octadecyl isocyanate (ODI), while its mechanical properties and thermal stability are enhanced significantly by adding two cost-effective and environmentally friendly particles, i.e., Cloisite Na^+ and biochar (BC). Our PCC insulation material showed the combined advantages of porosity, low density, hydrophobicity, robust mechanical stability, high thermal stability, and excellent thermal inertia, thus opening possibilities for applications in diverse areas, from building to transportation packaging insulation.

2. Materials and methods

2.1. Materials

Gum Tragacanth (GT) was provided by a local shop while being commercially available as well. It was thoroughly washed with ethanol, dried, and then milled to obtain a fine powder prior to any further use. Polyethylene glycol (PEG 6000) and octadecyl isocyanate (technical grade) were purchased from Sigma-Aldrich. Cloisite Na^+ was obtained from BYK Additives (Germany). Ethanol EtaxAa (highly pure ethanol, 99.5 %) was obtained from Altia Industrial (Finland). Biochar was prepared from softwood sawdust via pyrolysis at 700 °C under nitrogen gas in a tube furnace [26]. The carbonized wood sawdust was ground and sieved to a particle size below 50 μm prior to any further use.

2.2. Composite preparation and hydrophobization

A prescribed amount of PEG was dissolved in DI water at 50 °C. A known amount of GT powder was then added to the solution while raising the temperature to 80 °C under continuous stirring. The system was stirred for 24 h to get a clear viscose solution. The final solution was centrifuged at 2000 rpm (Thermo Scientific SL40FR Centrifuge) for 1 h to remove the bubbles and then lyophilized under a vacuum (Christ Alpha 2–4 Freeze Dryer) to get cryogel. The total solid content of both PEG and GT was fixed at 10 wt% in the solution. Three different compositions of each component were prepared, as summarized in Table 1, codded as PCC1 to PCC3. Preliminary testing confirmed PCC3 as the optimal composition regarding mechanical and thermal performances; as such, additives were added to this composition. The samples containing particles (nanoclay or biochar), named PCC3-C and PCC3-B series, were prepared with the same procedure except that, before dissolving PEG, the calculated amount of the particles was dispersed in DI water by 30 min sonication (SXSONIC probe sonicator). The preparation process is schematically shown in Fig. 1.

A simple solvent-free method was employed to make the PCC hydrophobic. The sample was first thoroughly vacuum-dried at 60 °C. Afterward, it was placed in a pre-heated desiccator containing a small amount of octadecyl isocyanate (ODI) (Fig. 1). The desiccator was then placed into an oven previously heated to 90 °C. The desiccator was kept for 8 h; then, the surface-coated PCC was removed, washed with DI water to eliminate unreacted isocyanate molecules, and dried at room temperature.

Table 1
The developed composite insulation formulation.

Composition	PEG (wt%)	GT (wt%)	Clay (wt%)	Biochar (wt%)
PEG	100	0	0	0
GT	0	100	0	0
PCC1	90	10	0	0
PCC2	80	20	0	0
PCC3	70	30	0	0
PCC3-B1	66.5	28.50	0	5
PCC3-B2	63	27	0	10
PCC3-C1	66.5	28.5	5	0
PCC3-C2	63	27	10	0

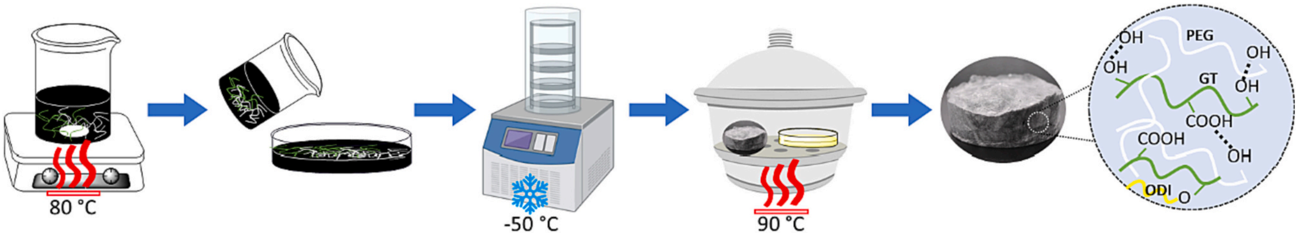

Fig. 1. Schematic representation of the PCC preparation process.

2.3. *Characterization*

2.3.1. *Porosity*

The porosity of the PCCs was measured based on the method reported in our previous work [27]. The cube PCC with specified dimensions was dried at 50 °C in a vacuum oven. It was weighted (m_d) and immersed in ethanol. After 48 h, it was taken out, its excess ethanol was removed with a blotting paper, and weighted again (m_s). The porosity (φ) was calculated using Eq. (1), in which V is the apparent volume of the sample and ρ is the ethanol density (789 kg m^{-3}). Each measurement was repeated five times, and the mean value ± standard deviation was reported.

$$\Phi = \frac{m_s - m_d}{\rho V} \tag{1}$$

2.3.2. *Scanning electron microscopy*

The microstructure of the PCCs was monitored with a Zeiss Sigma VP scanning electron microscope. The samples were coated with a thin layer (~ 4 nm) of gold before the subjection of imaging. The pore size was calculated using ImageJ software.

2.3.3. *Fourier transform infrared spectroscopy*

The chemical structure of the samples was studied on a Fourier transform infrared spectroscopy (FTIR) device (PerkinElmer FTIR with ATR model). The measurement was performed between 4000 cm^{-1} to 500 cm^{-1} with a scan rate of 16 and a resolution of 4 cm^{-1}.

2.3.4. *Contact angle measurement*

The contact angle of a water droplet was measured on Theta Flex optical tensiometer device at 25 °C. 5 μl water droplet was placed on the sample's surface, and two digital photographs of the droplet were captured immediately and 120 s after deposition.

2.3.5. *Compression test*

The compressive mechanical properties of the PCCs were evaluated on Universal Tester Instron 4204 machine. The cylinder-shaped samples were first conditioned for 72 h at temperature and relative humidity of 24 °C and 55 %, respectively. After that, they were subjected to the compressive force of 1 kN with a rate of 1 mm min^{-1}. Compressive modulus (tangent modulus at 1 % strain) and compressive strength at 30 % and 70 % strain were reported and discussed. Each measurement was repeated three times, and the mean value ± standard deviation was reported.

2.3.6. *Thermogravimetric analysis*

The thermal decomposition trend of the samples was monitored by thermogravimetric analysis (TGA) performed on TA Instruments TGA Q500. The samples were heated up from room temperature to 800 °C with a heating rate of 10 °C min^{-1} under a nitrogen atmosphere with a flow of 60 $ml.min^{-1}$.

2.3.7. *Differential scanning calorimetry*

The phase change properties of the PCCs were examined by differential scanning calorimetry (DSC) (TA Instruments Discovery DSC 250 Auto model). The samples were subjected to three heating-cooling cycles from −10 °C to 90 °C with a heating/cooling rate of 5 °C min^{-1} under a nitrogen atmosphere. The melting temperature (T_m), crystallization temperature (T_c), melting enthalpy (ΔH_m), and crystallization enthalpy (ΔH_c) were extracted from all cycles, and the mean values ± standard deviation were reported. The heating/cooling cycles were repeated 100 times on the optimum composition to examine the cyclability of phase change behavior.

2.3.8. *Thermal conductivity*

A TCi Thermal Conductivity Analyzer (C-Therm) using a modified transient plane source (MTPS) technique was used to measure the thermal conductivity of the PCCs. A disk-shaped geometry with a diameter of 30 mm was used.

2.3.9. *Thermal chamber and camera*

The insulation performance was measured in a thermal chamber under a temperature-controlled program to increase the temperature from room value to 70 °C. The measurement was conducted with water-filled bottles covered with the developed insulations. The thickness of the insulation was 12 mm in all samples. The results were compared with a bare bottle as well as a bottle covered with commercial polyethylene foam with thermal conductivity of 0.040–0.095 W m^{-1} K^{-1} and a bulk density of 100 Kg m^{-3} (based on the product data sheet) and a thickness of 12 mm (Fig. S2). Furthermore, a PCC sample was placed on a hot plate, and the temperature distribution images versus time were captured by a FLER SC7000 infrared thermal camera.

3. Results and discussion

3.1. *Morphological properties*

Highly porous structures with a low bulk density have been considered the core material for thermal insulation systems [28,29]. Thus, the porosity and bulk density of the developed PCCs were examined and summarized in Table 2. All samples revealed a relatively low bulk density ranging from 115 to 140 kg m^{-3} and high porosity within 73 to 88 %. Although the density range was higher than that of light foam-based insulation materials, such as expanded polystyrene or polyurethane foam, it was close to the reported values for glass and rock wool as well as plant-based insulations [16,17,19]. In the case of PCC1 to PCC3, the bulk density increased upon increasing the GT content,

Table 2
Physical and thermal properties of PCCs.

Sample	Density (kg m^{-3})	Porosity (%)	Mean pore size (μm)	Thermal conductivity (W m^{-1} K^{-1})
PCC1	113 ± 3	88 ± 3.5	–	–
PCC2	115 ± 5	85 ± 3.4	–	–
PCC3	119 ± 4	83 ± 3.3	130 ± 40	0.036 ± 0.001
PCC3-B1	121 ± 5	81 ± 3.1	85 ± 18	0.037 ± 0.002
PCC3-B2	126 ± 6	74 ± 3.0	28 ± 10	0.038 ± 0.002
PCC3-C1	124 ± 5	80 ± 2.9	33 ± 10	0.037 ± 0.001
PCC3-C2	134 ± 7	73 ± 3.0	104 ± 48	0.039 ± 0.001

which could be due to the higher bulk density of the GT powder than that of PEG. The bulk density slightly increased in PCC with the additives, which could be explained by the higher dry mass content. Noticeably, a linear trend was observed between the density and porosity of PCC, where the samples with higher bulk density revealed a lower porosity (Fig. S3), similar to that reported by Trambitski et al. [30].

SEM images in Fig. 2 were captured from the cross-section area of the PCCs to monitor their porosity and pore size. All samples possessed a typical three-dimensional porous architecture with open-cell microstructures, in which the irregular-shaped pores, characterized by interconnectivity and robust internal structure, were distributed evenly throughout the PCCs. The incorporation of BC or Cloisite Na$^+$ did not change the pore geometry considerably, yet consistent with the literature [31], the PCC with additives revealed a denser and more uniform microstructure compared with the particle-free samples. The average pore size decreased from 130 ± 40 μm for PCC3 to 28 ± 10 μm for PCC-B2 (Table 2), which could be due to its higher dry mass as well as its highly dense, robust, and well-developed network structures resulting in the creation of pores with smaller sizes [25,32]. Furthermore, no evidence of phase separation was observed in all PCCs, and the particles were distributed homogeneously in most PCCs. Only in the case of PCC3-C2 clay particles showed minor agglomeration, as spherical particles could be seen in the SEM image with a higher magnification (red arrow in Fig. 2f), and as a result, the pore size increased significantly to 104 ± 48 μm.

3.2. Chemical structure and surface properties

For the long-term application of thermal insulators, water resistance is essential so that the material can still maintain a low thermal conductivity in a humid environment. Besides, it is essential to deter the destruction of the porous insulation skeleton structure through water vapor absorption by the pores [33,34]. Due to the presence of abundant hydroxyl groups of GT, the hydrophilic nature of GT could be easily altered by using long-chain aliphatic molecules, e.g., ODI. In the current study, the hydrophobic modification was applied by coating the surface of PCCs with a thin layer of ODI molecules. FTIR was carried out to investigate the possible covalent bonding between the hydroxyl groups of the GT and the isocyanate group of ODI. FTIR spectra of the PCC3-B2 and PCC3-C2 before and after surface coating are depicted in Fig. 3a. Except for the hydroxyl groups' characteristic peak at 3400 cm^{-1}, the other main characteristic peaks were untouched after surface coating with ODI. The considerable reduction in the peak intensity at 3400 cm^{-1} suggested the consumption of hydroxy groups during the coating process. Besides, some new bands appeared after surface coating. Namely, two pronounced peaks formed at 2910 cm^{-1} and 2850 cm^{-1} regions that could be due to asymmetric and symmetric methylene groups in the alkyl chain of the coated ODI. Furthermore, two new bands appeared at 1615 cm^{-1} and 1580 cm^{-1}, which could be attributed to the amide I and amide II vibration peaks. The FTIR spectra confirm the reaction between isocyanate groups of ODI and hydroxyl groups of GT and PEG. Of note, the proper removal of ODI molecules after the washing was verified by the absence of any characteristic peaks in the region of 2270 cm^{-1}, which is assigned to the isocyanate group [35,36]. According to our previous experiments obtained from the elemental analysis, the amount of grafted ODI is around 10 wt% [35,36].

The FTIR spectra of initial components and PCCs, as well as a thorough peaks description, are provided in the Supplementary Information. All the characteristic peaks of the initial components were observed in the PCCs (Fig. S4), while their intensity slightly changed according to the portion of each component. No new characteristic bands appeared on the spectra of the PCCs, indicating the physical nature of the interactions between PEG and GT.

A water contact angle measurement was carried out further to explore the surface properties, i.e., the surface wettability of the PCCs after ODI coating. A contact angle greater than 90° is considered a hydrophobic solid surface in which the liquid is not easy to wet the solid. Besides, the larger the contact angle, the worse the material surface's wettability [37]. The photographs of the water droplet immediately and 120 s after deposition are provided in Fig. 3b to Fig. 3e. The contact angle was less than 90° before coating, while it increased to approximately 128° afterward, indicating a notable change in the surface properties. The coating of ODI on the surface of the PCC3-B2 insulation converted the surface from hydrophilic to hydrophobic. The water droplet formed a stable sphere on the surface of the ODI-coated sample, which was well preserved even after 120 s (Fig. 3e). Unlike the coated sample, the water droplet was absorbed in 10 s in the uncoated insulation (Fig. 3c), showing its high hydrophilic surface property. A routine water absorption test was also performed to evaluate the water retention capacity of the PCC3-B2 insulation before and after coating. While the uncoated insulation disintegrated in water within 60 min, the ODI-coated one maintained well even after a week (Fig. 5) with minor water absorption of 3.6 ± 0.3 %. Altogether, the contact angle measurement, along with the water absorption study, confirmed that the ODI coating was favorable for the water resistance performance of the PCCs, which could be due to its low polar long aliphatic chains.

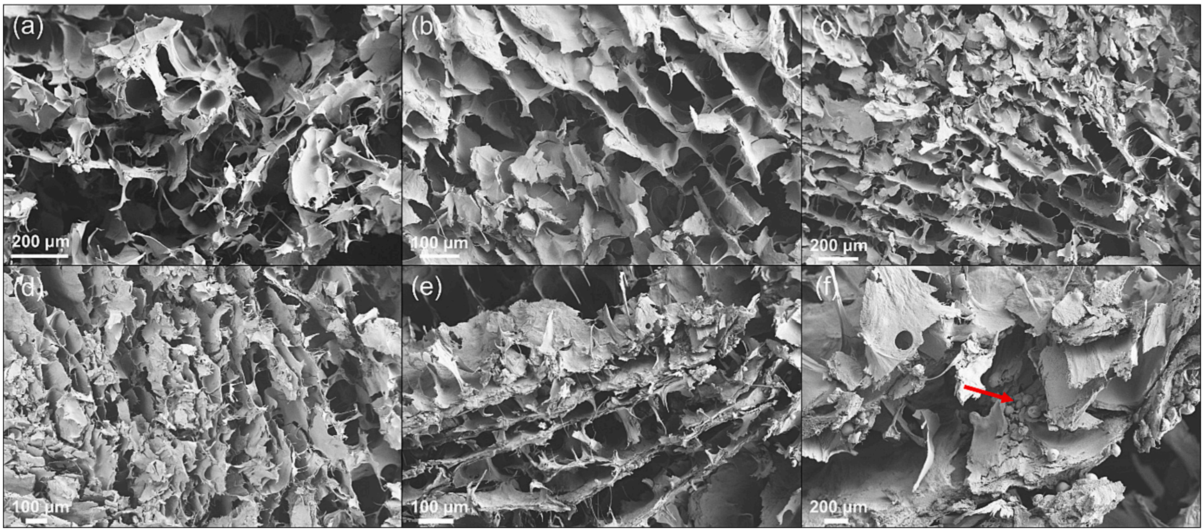

Fig. 2. SEM images of a) PCC3, b) PCC3-B1, c) PCC3-B2, d) PCC3-C1, and e) and f) PCC3-C2.

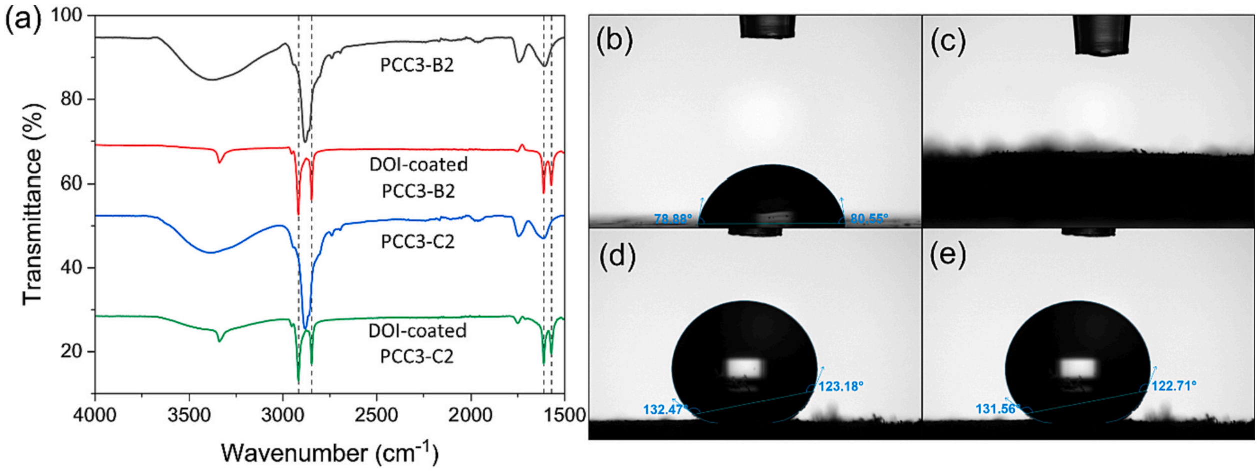

Fig. 3. FTIR spectra of a) PCC3-B2 and PCC3-C2 before and after surface coating with ODI. The photographs of the water droplet in the air on the surface of PCC3-B2 b) and c) before and d) and e) after coating with ODI. b) and d) was captured immediately after droplet deposition, and c) and e) 120 s after deposition.

3.3. *Mechanical resilience*

For insulating materials, the elastic behavior, reflected by compressive strength and modulus, is of great significance due to its direct effect on the insulating properties [38]. Hence, the compressive properties of the developed PCCs, i.e., the compressive modulus and compressive strength at 30 % and 70 % strain, were examined. The typical compressive stress-strain curves, as well as the comparison of different compressive properties, are depicted in Fig. 4. All formulations had good stability without any visual fracture throughout the test. They presented a linear viscoelastic behavior at low strain rates, afterward a relatively large plateau region, and finally, a densification zone. This trend was consistent with the compression behavior of open-cell porous materials and suggested a flexible deformation pattern of the developed insulations [16,39]. Both compressive modulus and compressive strength increased significantly with increasing GT content. Furthermore, adding the particles, i.e., Cloisite Na$^+$ and BC, notably improved the compressive properties. For instance, the compressive modulus increased from 5.3 ± 0.4 MPa in PCC1 to 6.6 ± 0.5 MPa in PCC3 and further enhanced to 11.1 ± 0.9 MPa in PCC3-B2. Similarly, the compressive strength at 70 % strain improved from 72 ± 4 kPa in PCC1 to 317 ± 11 kPa and 702 ± 21 kPa in PCC3 and PCC3-B2, respectively. Such improvement in compressive performance could be due to the increase in density and reduction in porosity upon increasing the portion of GT and adding particles. Moreover, it could be attributed to the uniform dispersion of the particles with higher rigidity and their good compatibility with the polymer matrix that strengthen the cell walls and structure [16,39]. The improved network regularity and the degree of crosslinking freedom, and the decrease in the polymer chains' flexibility could be other reasons to enhance mechanical performance [31,40]. To conclude, the observed compressive properties of the composite insulations in the current study were in good agreement with those reported for bio-based composites containing clay [41,42] or biochar [31,43]. Besides, they were in line with the compressive properties of the expanded polystyrene foam [38,44,45], as well as polyurethane foam [46,47], making them potential candidates for insulated packaging materials.

3.4. *Thermogravimetric analysis*

The thermal stability of the polymeric composites can be increased by incorporating fillers and additives [48]. The thermal decomposition of PCCs, as well as the initial materials, were monitored by TGA in a nitrogen atmosphere to investigate the effect of additives, i.e., BC and Cloisite Na$^+$, on the thermal stability of the developed PCCs. The TGA/DTG thermograms are depicted in Fig. 5, and the corresponding data, including the 5 % ($T_{5\%}$), 10 % ($T_{10\%}$), and maximum decomposition temperatures (T_{max}), as well as the char residue at 800 °C, are summarized in Table 3. The plain PEG presented one sharp mass loss step that started at approximately 210 °C and ended at about 410 °C with a T_{max} of 395 °C, like that reported by Zhao et al. [11] and Wang et al. [49], who used plain PEG with the same molecular weight. GT showed two pronounced mass loss regions, an approximately 10 % mass loss below 200 °C attributed to the release of the hydroxyl groups, followed by a considerable mass loss of approximately 65 % assigned to the

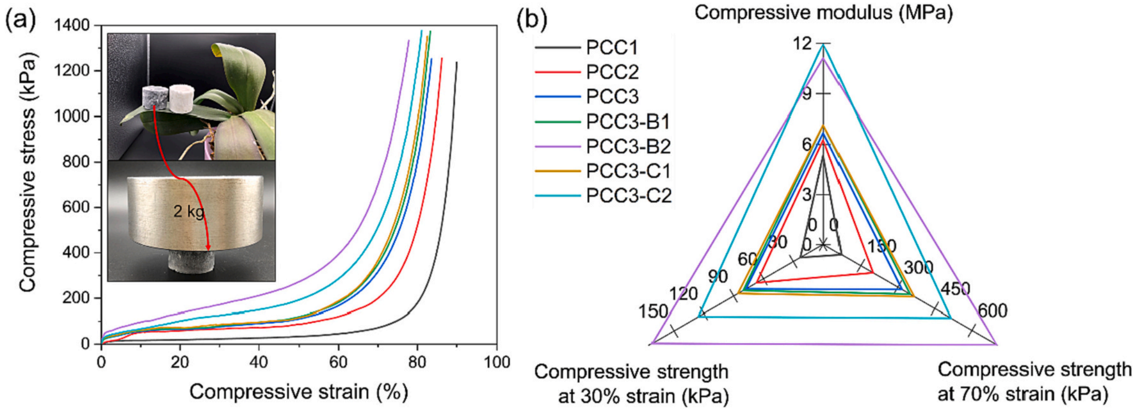

Fig. 4. a) Compressive stress-strain curves and b) the comparison between the compressive mechanical properties.

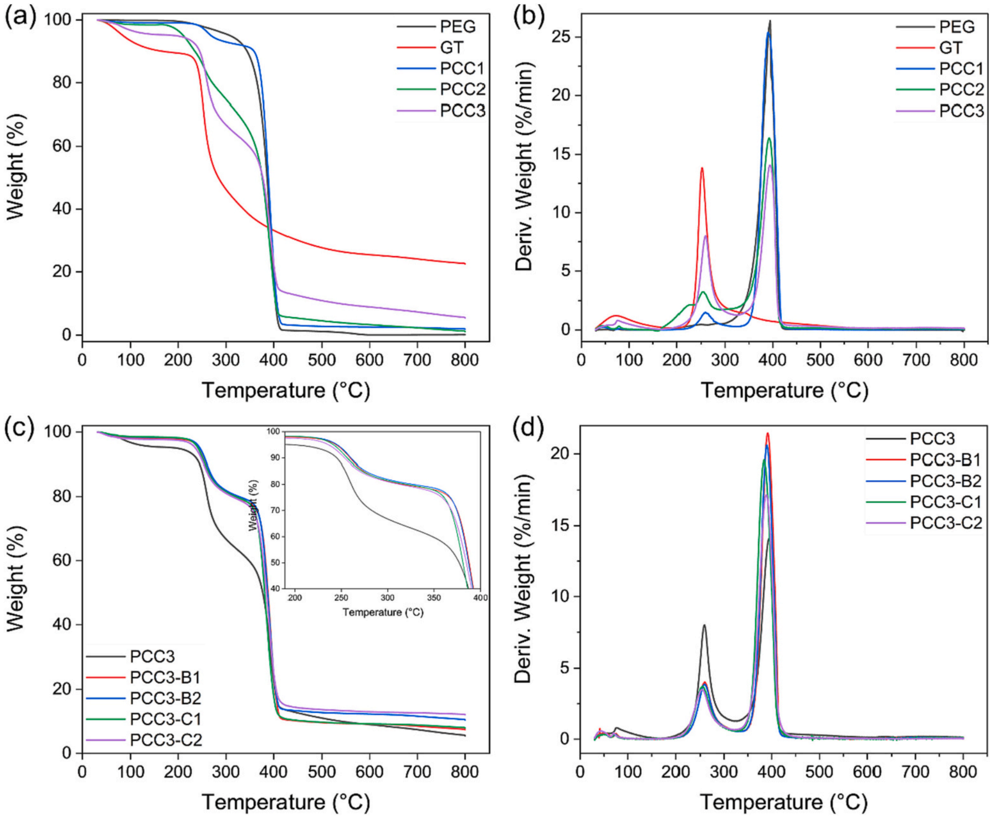

Fig. 5. TGA/DTG thermograms of a,b) PEG, GT, and PCCs with no additives, and c,d) PCCs with additives under a nitrogen atmosphere.

Table 3
TGA and DSC results.

Code	$T_{5\%}$ (°C)	$T_{10\%}$ (°C)	T_{max} (°C)	Char residue (%)	T_m (°C)	ΔH_m (J g^{-1})	ΔH_c (J g^{-1})	T_C (°C)
PEG	309.1	344.5	394.9	0.2	57.4	185.3	172.6	34.5
GT	76.2	136.6	251.1	25.3	–	–	–	–
PCC1	269.1	358.9	390.3	3.5	56.5	160.1	151.9	33.3
PCC2	210.7	234.9	392.8	2.8	57.5	136.2	132.0	38.5
PCC3	195.3	244.9	393.8	6.2	56.8	106.9	104.8	36.5
PCC3-B1	244.1	259.2	391.5	9.2	56.5	100.0	96.3	39.3
PCC3-B2	245.3	260.2	389.3	12.6	58.1	110.5	104.5	39.8
PCC-C1	241.2	256.1	383.6	10.0	57.8	112.0	106.6	36.8
PCC-C2	235.9	253.3	388.1	14.2	51.8	97.5	95.6	28.9

decomposition of the polysaccharide backbone [50]. As expected, PCC presented three mass loss regions, two of which were due to the GT portion and the third to the PEG portion. Furthermore, the intensity of the decomposition DTG peaks changed in proportion to the concentration of the components, i.e., PEG and GT.

Although T_{max} did not change significantly after the presentation of BC or Cloisite Na^+, $T_{5\%}$ and $T_{10\%}$ showed a shift. For instance, $T_{5\%}$ and $T_{10\%}$ increased from 195 °C and 245 °C in the PCC3, respectively, to 245 °C and 260 °C in the PCC composed of 10 wt% BC. The same trend could be seen for the PCC containing Cloisite Na^+. These results revealed that the weight losses in the composite insulations started at higher temperatures than the plain PCC3, and adding the particles lowered the decomposition rate and improved the thermal stability. Likewise, the char residue increased considerably in the composites, indicating that the decomposition of polymers was hindered by the particles, and they enhanced the thermal stability [51,52]. As shown in Fig. S6, both BC and Cloisite Na^+ had platelet structures; therefore, they could form an effective diffusion barrier, acting as a thermal insulator and shielding combustible products from heat during thermal decomposition [48,53]. The increased heterogeneity of the composite structure compared to the composition with no additives, morphology optimization of char layers, mechanical reinforcement, and preventing or reducing dripping behavior have been reported as other reasons for the observed higher thermal stability in the high aspect ratio particle/polymer blends [54–56]. Overall, both BC and Cloisite Na^+ improved the thermal property of the PCCs in terms of the delay of decomposition temperatures and displayed great potential and benefits in preparing high thermal stability materials, as previously reported in other composites [57]. Notably, the BC-incorporated insulation presented higher thermal stability than the clay-incorporated one, which could be explained by the better thermal stability of BC than Cloisite Na^+ (Fig. S7). Of note, the slightly lower thermal stability of PCC3-C2 than PCC3-C1 could be explained by the partial aggregation of the clay particles at a high loading of 10 wt% [58,59], as previously proved in SEM images.

3.5. *Phase change properties*

DSC studies were performed to evaluate the PCCs' phase change properties, including melting temperature (T_m), melting enthalpy (ΔH_m), crystallization temperature (T_c), and crystallization enthalpy (ΔH_c), as reported in Table 3 and Fig. 6. Pure PEG showed T_m and T_c at 57.4 °C and 34.5 °C, with 185.2 J g^{-1} and 176.3 J g^{-1} melting and crystallization enthalpy values, respectively. Like the plain PEG, the PCCs showed one melting and one crystallization peak. Thus, GT only served as a supporting matrix and did not restrict the normal phase change process of PEG in the composite. Although both T_m and T_c did not change significantly, the corresponding enthalpies were reduced proportionally to the decrease in the PEG portion, likewise with the results reported for PEG-based phase change materials [10,60]. For example, the melting and crystallization enthalpies decreased from 160 J g^{-1} and 152 J g^{-1} for the composition with 90 % PEG to 106.9 J g^{-1} and 104.8 J g^{-1} for the formulation with 70 % PEG. The lowest enthalpy values were seen for PCC3-C2, which could be attributed to the smaller portion of PEG compared with the rest of the compositions, as well as the binding of intermolecular hydrogen bonds that can prevent the movement of ether chain and crystalline area of the PEG segments [61]. Surprisingly, for the PCC3-B2 and PCC-C1 formulations, the phase change enthalpies were slightly higher than the particle-free sample, i.e., PCC3. These insulations seemed to provide an optimal pore structure that could hold more PEG than the other samples [62]. Furthermore, the DSC of PCC3-B2 before and after ODI coating showed insignificant differences (Fig. S8). Briefly, DSC thermograms supported that the phase change enthalpies of the developed PCCs were promising for creating high-performance PCM systems in the field of thermal management [15].

To investigate the possibility of PEG leakage, the PCC3 and PCC3-B2 insulations were kept in an oven at 80 °C for 2 h and then subjected to DSC testing. The DSC curves are depicted in Fig. 7a. Furthermore, a thermal cycling test, in which the melting and solidification scans were repeated 100 times, was performed to study the phase transition stability of the PCC3-B2 insulation. The 1st and 100th cycles are provided in Fig. 7b, and the whole heating-cooling cycles are depicted in Fig. S9. Moreover, the measured phase change properties before and after the cycling test are tabulated in Table 4. It is obvious that the phase transition enthalpy did not show a noticeable change after heat treatment at 80 °C, indicating there was no leakage or loss of the PCM [63]. In other words, PEG was effectively kept in the porous structure of the GT matrix. The absence of the PEG leakage could also be observed from the photographs captured from the insulations before and after heat treatment at 80 °C (Fig. 7c and Fig. S10). On the other side, the DSC curve of the PCC3-B2 insulation did not change after the heating/cooling cycles. Compared to the 1st cycle, after the 100th cycle, the enthalpies just slightly decreased; namely, a 5.7 % decrease in the enthalpy of melting and the 3.3 % decrease in the crystallization enthalpy. These small reductions could be due to the increasing nonactive PCM caused by intermolecular interactions that become more profound by the continuous rapid temperature change [64,65]. The FT-IR spectra of the PCC3-B2 before and after cycling are compared in Fig. S11 to provide more evidence for stability. As can be seen, no considerable difference could be detected between the spectra before and after cycling, indicating no PEG leakage and significant stability of the developed PCM insulation even after 100 times cooling/heating cycles. All in all, the developed PCM not only presented phase transition stability but also possessed excellent cycle stability, ensuring the ability to adjust the road temperature over a lengthy period of time.

3.6. Thermal insulation performance

The thermal insulation performance of the composite insulations was tested with a water bottle covered with a 12 mm insulation layer, as depicted in Fig. 8b. The changes in water temperature inside the bottle were investigated in a thermal chamber upon heating from room temperature to 70 °C and a consequent cooling back to room temperature. The results are plotted in Fig. 8a. As can be seen, the bare bottle temperature rose continuously and reached the maximum value of 68 °C in 45 min. However, the temperature increased at a lower rate in the

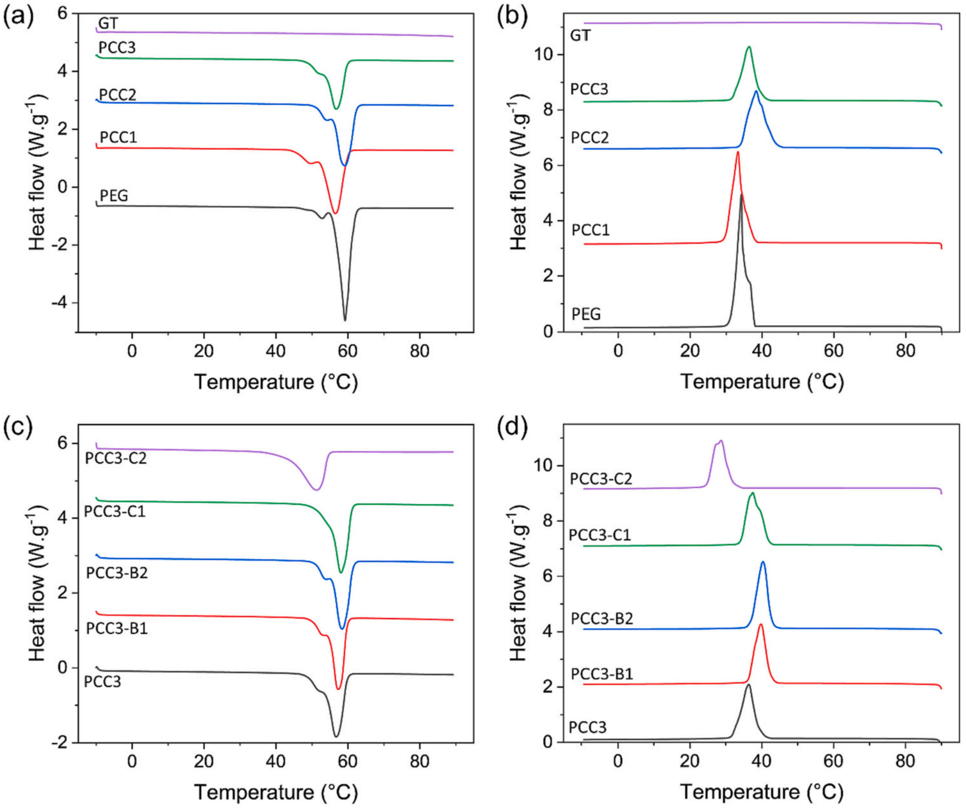

Fig. 6. DSC thermograms of the plain PEG, GT, and PCCs. a) and c) second heating cycles and b) and d) second cooling cycles.

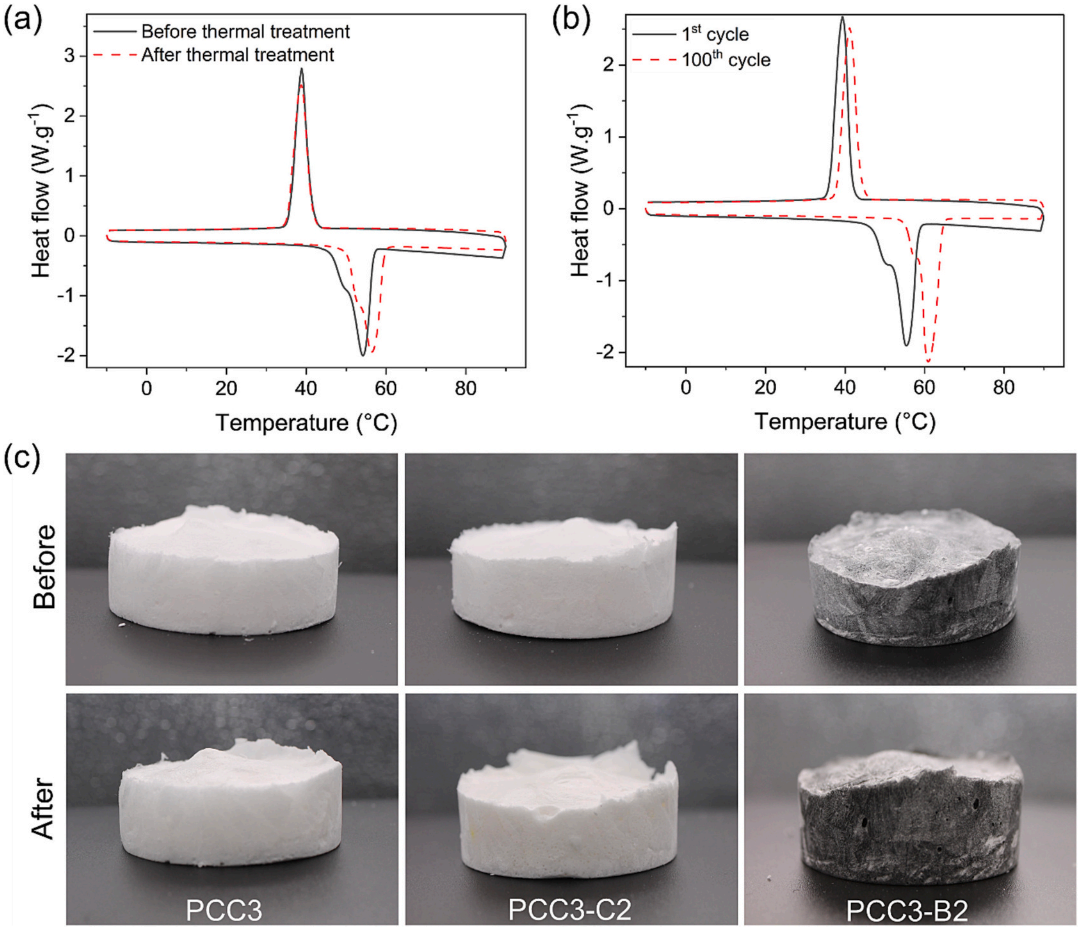

Fig. 7. DSC thermograms of PCC3-B2 insulation: a) before (solid line) and 2 h after (dash line) heating treatment at 90 °C and b) the 1st (solid line) and the 100th (dash line) cycles. c) the photograph of the developed PCCs before and after heating treatment above PCM's melting temperature at 80 °C.

Table 4
PCC3-B2 phase change properties.

Sample's condition	T_m (°C)	ΔH_m (J g^{-1})	ΔH_c (J g^{-1})	T_C (°C)
Before thermal treatment[a]	54.1	112.1	107.3	39.3
After thermal treatment[a]	56.4	108.3	105.2	39.2
1st heating-cooling cycle	55.3	111.3	106.8	39.2
100th heating-cooling cycle	60.7	104.9	103.2	40.8

[a] The data extracted from the first heating/cooling cycle.

covered bottles, and the maximum temperature was considerably lower. For instance, it was 50 °C in the bottle covered with commercial PE foam and 44 °C in the bottles covered with our PCC insulations. The results strongly showed the benefit of insulations, especially the developed ones in the current study, enabling consistent prevention of thermal shocks or transients arising from sudden temperature changes in the surrounding environment. Similar performance was previously observed with cellulosic PCM composites [64]. It is worth mentioning that the high thermal insulation properties of the PCCs were consistent with their low thermal conductivity values, which ranged from 0.035 to 0.038 W m^{-1} K^{-1} (Table 2). Biopolymeric foams and aerogels are known for their low thermal conductivity within the 0.020 and 0.040 W m^{-1} K^{-1} range [66,67]. Nevertheless, by comparing the thermal conductivity of the composite insulations with the commercial PE, it could be found that the higher performance of the developed insulations was not only due to their low thermal conductivity but also attributed to the incorporation of PEG, acting as an energy-storage material. To conclude, our lightweight composite insulations could be considered promising alternatives for fossil-based insulations in eco-friendly and energy-efficient applications, thanks to the low conductivity of the biopolymer (GT) and the high thermal inertia of the PCM (PEG).

The temperature distribution images of the PCC sample placed on a hot plate are given in Fig. 8d and Fig. S12. It can be observed that heat was transferred very slowly within the material, even when it was placed in direct contact with a hot object. This is consistent with the thermal conductivity values and the water bottle test. After removing the heating source, the middle of the sample could hold the absorbed heat (Fig. S12).

4. Conclusions

In this study, we developed a series of bio-based insulation materials consisting of gum tragacanth (GT) biopolymer and polyethylene glycol (PEG) phase change material (PCM). Additionally, biochar (BC) and Cloisite Na$^+$ additives were incorporated to enhance their mechanical strength and thermal stability. The phase change composite (PCC) was then covered with a thin layer of octadecyl isocyanate (ODI) to alter its surface properties from hydrophilic to hydrophobic. The PCCs possessed a low-density porous structure (up to 88 %) with very low thermal conductivity (0.035 W K^{-1} m^{-1}). Furthermore, the formulations composed of BC and Cloisite Na$^+$ revealed robust mechanical stability under compression, as well as good thermal stability. After ODI coating, the wettability and water uptake capacity of the composite was minor, demonstrated by the water droplet contact angle and water impression test. The PCCs provided leakage-free phase transition enthalpy up to 160 J g^{-1} and excellent cycling stability, ensuring the ability to adjust road temperature over a long period. Overall, our PCC provides all the

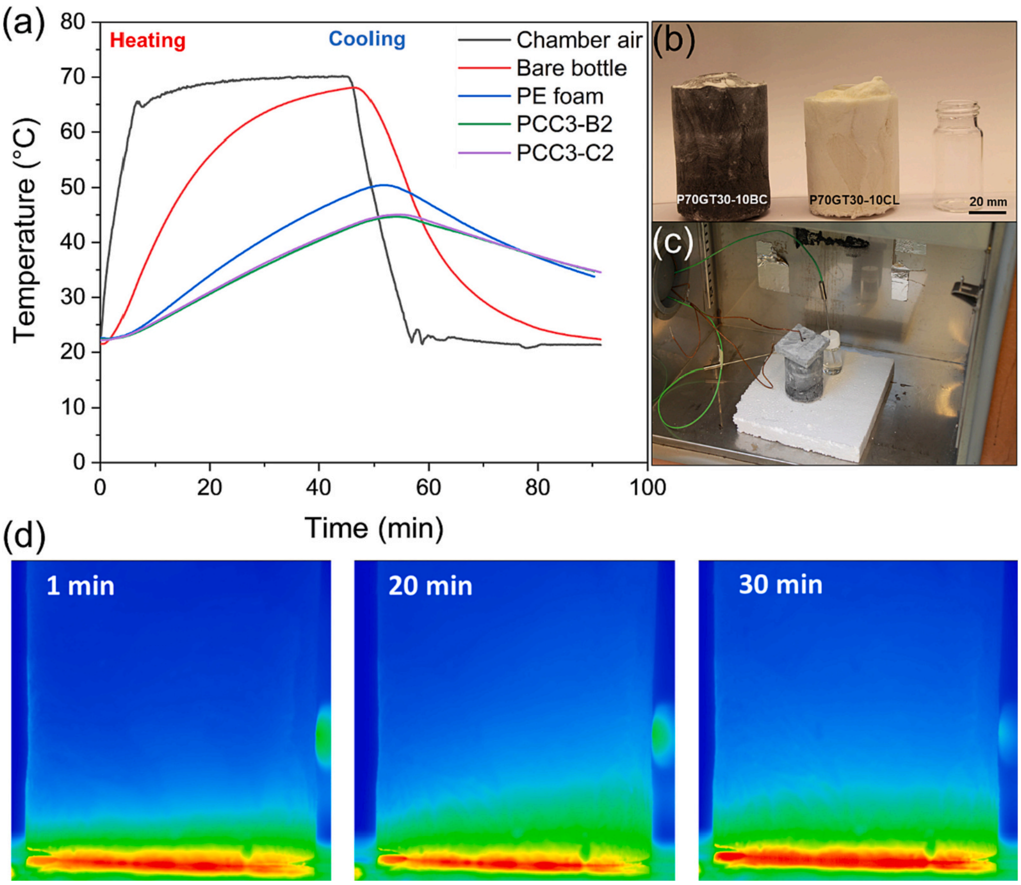

Fig. 8. a) Thermal insulation performance of PCC based on the temperature changes of water inside the bottle versus time in a thermal chamber test. The photographs of the b) bare bottle and insulated covered bottles, and c) inside the thermal chamber. d) Temperature distribution images of a PCC sample placed on a hot plate in 1, 20, and 30 min. The temperature graphs are included in Fig. S11.

necessary properties of excellent insulation, such as high porosity, low density, hydrophobicity, robust and mechanical stability, as well as thermal inertia and enthalpy of PCM. These make PCC an excellent candidate for many temperature- and energy-sensitive applications, including insulation packaging materials.

CRediT authorship contribution statement

Hossein Baniasadi: Conceptualization, Investigation, Methodology, Formal analysis, Visualization, Writing – original draft. **Jukka Seppälä:** Resources, Writing – review & editing, Funding acquisition. **Ari Kankkunen:** Methodology, Writing – review & editing. **Ari Seppälä:** Resources, Writing – review & editing. **Maryam Roza Yazdani:** Conceptualization, Investigation, Methodology, Formal analysis, Visualization, Resources, Writing – original draft, Funding acquisition.

Declaration of competing interest

The authors declare that there is no conflict of interest.

Data availability

Data will be made available on request.

Acknowledgment

The authors would like to acknowledge the funding of Business Finland (7428/31/2022, PCMI project) and the Academy of Finland; No. 343192 (SoMa), No. 327248 (ValueBiomat), and No. 327865 (Bioeconomy).

Appendix A. Supplementary data

Supplementary data to this article can be found online at https://doi.org/10.1016/j.est.2023.106725.

References

[1] W. Chalco-Sandoval, M.J. Fabra, A. López-Rubio, J.M. Lagaron, Development of polystyrene-based films with temperature buffering capacity for smart food packaging, J. Food Eng. 164 (2015) 55–62.
[2] C.E. Tas, H. Unal, Thermally buffering polyethylene/halloysite/phase change material nanocomposite packaging films for cold storage of foods, J. Food Eng. 292 (2021), 110351.
[3] M. Jafarpour, M. Fathi, N. Soltanizadeh, Encapsulation of polyethylene glycol as a phase change material using alginate microbeads to prevent temperature fluctuation-case study: fish packaging, Food Hydrocoll. 134 (2023) 1–7, 108029.
[4] A.M. Papadopoulos, State of the art in thermal insulation materials and aims for future developments, Energy Build. 37 (2005) 77–86.
[5] P. Arumugam, V. Ramalingam, P. Vellaichamy, Optimal positioning of phase change material and insulation through numerical investigations to reduce cooling loads in office buildings, J. Energy Storage 52 (2022), 104946.
[6] Z. Rahimpour, G. Verbič, A.C. Chapman, Can phase change materials in building insulation improve self-consumption of residential rooftop solar? An Australian case study, Renew. Energy 192 (2022) 24–34.
[7] T. Wang, X. Qiu, X. Chen, L. Lu, B. Zhou, Sponge-like form-stable phase change materials with embedded graphene oxide for enhancing the thermal storage efficiency and the temperature response in transport packaging applications, Appl. Energy 325 (2022), 119832.
[8] W. Chalco-Sandoval, M.J. Fabra, A. López-Rubio, J.M. Lagaron, Use of phase change materials to develop electrospun coatings of interest in food packaging applications, J. Food Eng. 192 (2017) 122–128.
[9] J. Weng, D. Ouyang, X. Yang, M. Chen, G. Zhang, J. Wang, Alleviation of thermal runaway propagation in thermal management modules using aerogel felt coupled

with flame-retarded phase change material, Energy Convers. Manag. 200 (2019), 112071.

[10] S. Tanwar, R. Kaur, Fabrication and investigation on influence of metal oxide nanoparticles on thermal, flammability and UV characteristics of polyethylene glycol based phase change materials, J. Energy Storage 54 (2022), 105318.

[11] S. Zhao, J. Li, S. Song, Preparation of porous titanium dioxide foam impregnated with polyethylene glycol as shape-stable composite phase change materials, J. Energy Storage 51 (2022), 104416.

[12] A.A. Aydın, H. Okutan, Polyurethane rigid foam composites incorporated with fatty acid ester-based phase change material, Energy Convers. Manag. 68 (2013) 74–81.

[13] V. Selvaraj, H. Krishnan, Acidic functionalized graphene dispersed polyethylene glycol nano-phase change material for the active cooling of a simulated heat-generating electronic system, J. Energy Storage 45 (2022), 103774.

[14] D.-L. Feng, Y.-Y. Zang, P. Li, Y.-H. Feng, Y.-Y. Yan, X.-X. Zhang, Polyethylene glycol phase change material embedded in a hierarchical porous carbon with superior thermal storage capacity and excellent stability, Compos. Sci. Technol. 210 (2021), 108832.

[15] S. Li, J. Li, Y. Liao, S. Chen, Y. Zheng, M. Li, K. Sun, Dual-functional polyethylene glycol/graphene aerogel phase change composites with ultrahigh loading for thermal energy storage, J. Energy Storage 54 (2022), 105337.

[16] Y. Guo, S. Zhang, G. Wang, Y. Zhu, Fabrication of anisotropic polyphosphazene/bio-based poly (urethane-acrylate) composite foams with high thermal insulation and flame retardancy, Polymer 231 (2021), 124108 (Guildf).

[17] C.H. Koh F. Gauvin K. Schollbach J. Brouwers Investigation of Material Characteristics and Hygrothermal Performances of Different Bio-Based Insulation Composites, Available SSRN 4128574. (n.d.).

[18] M. Khoukhi, A.D. Saleh, A.F. Mohammad, A. Hassan, S. Abdelbaqi, Thermal performance and statistical analysis of a new bio-based insulation material produced using grain puffing technique, Constr. Build. Mater. 345 (2022), 128311.

[19] F. Fedorik, J. Zach, M. Lehto, H.-R. Kymäläinen, R. Kuisma, M. Jallinoja, K. Illikainen, S. Alitalo, Hygrothermal properties of advanced bio-based insulation materials, Energy Build. 253 (2021), 111528.

[20] O. Duman, H. Uğurlu, C.Ö. Diker, S. Tunç, Fabrication of highly hydrophobic or superhydrophobic electrospun PVA and agar/PVA membrane materials for efficient and selective oil/water separation, J. Environ. Chem. Eng. 10 (2022), 107405.

[21] J. Shao, W. Sheng, C. Wang, Y. Ye, Solvent-free fabrication of tough self-crosslinkable short-fluorinated copolymer nanocoatings for ultradurable superhydrophobic fabrics, Chem. Eng. J. 416 (2021), 128043.

[22] C. Xu, C. Sun, H. Wan, H. Tan, J. Zhao, Y. Zhang, Microstructure and physical properties of poly (lactic acid)/polycaprolactone/rice straw lightweight bio-composite foams for wall insulation, Constr. Build. Mater. 354 (2022), 129216.

[23] N. Niknia, R. Kadkhodaee, Gum tragacanth-polyvinyl alcohol cryogel and xerogel blends for oral delivery of silymarin: structural characterization and mucoadhesive property, Carbohydr. Polym. 177 (2017) 315–323.

[24] N. Niknia, R. Kadkhodaee, Factors affecting microstructure, physicochemical and textural properties of a novel gum tragacanth-PVA blend cryogel, Carbohydr. Polym. 155 (2017) 475–482.

[25] M. Dehghan-Niri, E. Vasheghani-Farahani, M.B. Eslaminejad, M. Tavakol, F. Bagheri, Physicomechanical, rheological and in vitro cytocompatibility properties of the electron beam irradiated blend hydrogels of tyramine conjugated gum tragacanth and poly (vinyl alcohol), Mater. Sci. Eng. C 114 (2020), 111073.

[26] O. Tomin, M.R. Yazdani, Production and characterization of porous magnetic biochar: before and after phosphate adsorption insights, J. Porous. Mater. 29 (2022) 849–859.

[27] H. Baniasadi, R. Ajdary, J. Trifol, O.J. Rojas, J. Seppälä, Direct ink writing of Aloe vera/cellulose nanofibrils bio-hydrogels, Carbohydr. Polym. 118114 (2021).

[28] K. Li, G.M. Veith, M.E. Lamm, A. Stevens, T. Lamichhane, W. Guo, S.M. Mahurin, K. Biswas, D. Hun, H. Wang, Hermetically sealed porous-wall hollow microspheres enabled by monolithic glass coatings: potential for thermal insulation applications, Vacuum 195 (2022), 110667.

[29] Z. Wang, H. Gao, H. Liu, L. Liao, L. Mei, G. Lv, G. Zhu, D. Huang, Inorganic thermal insulation material prepared from pitchstone, J. Build. Eng. 32 (2020), 101745.

[30] Y. Trambitski, O. Kizinievič, V. Kizinievič, Modification of clay materials with retrograded starch hydrogel, Constr. Build. Mater. 314 (2022), 125619.

[31] Y. Guo, X. Liu, S. Xie, H. Liu, C. Wang, L. Wang, 3D ZnO modified biochar-based hydrogels for removing U (VI) in aqueous solution, Colloids Surf.A Physicochem. Eng. Asp. 642 (2022), 128606.

[32] J. Varshosaz, Z.S. Sajadi-Javan, M. Kouhi, M. Mirian, Effect of bassorin (derived from gum tragacanth) and halloysite nanotubes on physicochemical properties and the osteoconductivity of methylcellulose-based injectable hydrogels, Int. J. Biol. Macromol. 192 (2021) 869–882.

[33] J. Gu, R. Fu, S. Kang, X. Yang, Q. Song, C. Miao, M. Ma, Y. Wang, H. Sai, Robust composite aerogel beads with pomegranate-like structure for water-based thermal insulation coating, Constr. Build. Mater. 341 (2022), 127722.

[34] M. Cao, S.-L. Li, J.-B. Cheng, A.-N. Zhang, Y.-Z. Wang, H.-B. Zhao, Fully bio-based, low fire-hazard and superelastic aerogel without hazardous cross-linkers for excellent thermal insulation and oil clean-up absorption, J. Hazard. Mater. 403 (2021), 123977.

[35] H. Baniasadi, J. Trifol, S. Lipponen, J. Seppälä, Sustainable composites of surface-modified cellulose with low–melting point polyamide, Mater. Today Chem. 22 (2021), 100590.

[36] H. Baniasadi, S. Lipponen, M. Asplund, J. Seppälä, High-concentration lignin biocomposites with low-melting point biopolyamide, Chem. Eng. J. 451 (2023), 138564. https://doi.org/10.1016/j.cej.2022.138564.

[37] S. Wang, L. Liu, H. Li, S. Zou, G. Zhang, Experimental research on waterproof enhanced biomass-based building insulation materials, Energy Build. 252 (2021), 111392.

[38] J. Zhao, G. Wang, W. Zhu, Z. Xu, A. Zhang, G. Dong, G. Zhao, Ultra-light, super-insulating, and strong polystyrene/carbon nanofiber nanocomposite foams fabricated by microcellular foaming, Eur. Polym. J. 173 (2022) 1–7, 111261.

[39] S. Wu, D. Chen, G. Zhao, Y. Cheng, B. Sun, X. Yan, W. Han, G. Chen, X. Zhang, Controllable synthesis of a robust sucrose-derived bio-carbon foam with 3D hierarchical porous structure for thermal insulation, flame retardancy and oil absorption, Chem. Eng. J. 434 (2022), 134514.

[40] M.E. El-Naggar, S. Gaballah, G. Abdel-Maksoud, H.S. El-Sayed, A.M. Youssef, Preparation of bactericidal zinc oxide nanoparticles loaded carboxymethyl cellulose/polyethylene glycol cryogel for gap filling of archaeological bones, J. Mater. Res. Technol. 20 (2022) 114–127.

[41] S. Sezen, V.K. Thakur, M.M. Ozmen, Highly effective covalently crosslinked composite alginate cryogels for cationic dye removal, Gels 7 (2021) 178.

[42] M. Falakaflaki, J. Varshosaz, M. Mirian, Local delivery of usnic acid loaded rhamnolipid vesicles by gelatin/tragacanth gum/montmorillonite/vanillin cryogel scaffold for expression of osteogenic biomarkers and antimicrobial activity, J. Drug Deliv. Sci. Technol. 69 (2022), 103147.

[43] Z. Wu, X. Chen, B. Yuan, M.-L. Fu, A facile foaming-polymerization strategy to prepare 3D MnO2 modified biochar-based porous hydrogels for efficient removal of Cd (II) and Pb (II), Chemosphere 239 (2020), 124745.

[44] P.M. Fard, M.G. Alkhansari, Innovative fire and water insulation foam using recycled plastic bags and expanded polystyrene (EPS), Constr. Build. Mater. 305 (2021), 124785.

[45] M.-E. Li, H.-B. Zhao, J.-B. Cheng, T. Wang, T. Fu, A.-N. Zhang, Y.-Z. Wang, An effective green porous structural adhesive for thermal insulating, flame-retardant, and smoke-suppressant expandable polystyrene foam, Engineering (2022), 114-127151-160.

[46] L. Hou, H. Li, Y. Liu, K. Niu, Z. Shi, L. Liang, Z. Yao, C. Liu, D. Tian, Synergistic effect of silica aerogels and hollow glass microspheres on microstructure and thermal properties of rigid polyurethane foam, J. Non-Cryst. Solids 592 (2022), 121753.

[47] C. Li, H. Ye, S. Ge, Y. Yao, B. Ashok, N. Hariram, H. Liu, H. Tian, Y. He, G. Guo, Fabrication and properties of antimicrobial flexible nanocomposite polyurethane foams with in situ generated copper nanoparticles, J. Mater. Res. Technol. 17 (2022) 3603–3615.

[48] X. Zhou, Q. Fu, Z. Zhang, Y. Fang, Y. Wang, F. Wang, Y. Song, C.U. Pittman Jr., Q. Wang, Efficient flame-retardant hybrid coatings on wood plastic composites by layer-by-layer assembly, J. Clean. Prod. 321 (2021), 128949.

[49] C. Wang, Z. Huang, T. Wang, X. Liu, P. Zhu, Light-thermal-electric energy conversion based on polyethylene glycol infiltrated carboxymethylcellulose sodium-derived carbon aerogel, Energy Convers. Manag. 267 (2022), 115948.

[50] K. Dixit, S. Kulanthaivel, T. Agarwal, K. Pal, S. Giri, T.K. Maiti, I. Banerjee, Gum tragacanth modified nano-hydroxyapatite: an angiogenic-osteogenic biomaterial for bone tissue engineering, Ceram. Int. 48 (2022) 14672–14683.

[51] T. Perroud, V. Shanmugam, R.A. Mensah, L. Jiang, Q. Xu, R.E. Neisiany, G. Sas, M. Försth, N.K. Kim, M.S. Hedenqvist, Testing bioplastics containing functionalised biochar, Polym. Test. 107657 (2022).

[52] T.G. Weldemhret, H.G. Menge, D.-W. Lee, H. Park, J. Lee, J. Il Song, Y.T. Park, Facile deposition of environmentally benign organic-inorganic flame retardant coatings to protect flammable foam, Prog. Org. Coat. 161 (2021), 106480.

[53] G. Viscusi, S. Liparoti, R. Pantani, G. Barra, G. Gorrasi, A layer-by-layer approach based on APTES/Cloisite to produce novel and sustainable high performances materials based on hemp fiberboards, Polym. Degrad. Stab. 198 (2022), 109892.

[54] M. Abd El-Fattah, A.M. El Saeed, M.M. Dardir, M.A. El-Sockary, Studying the effect of organo-modified nanoclay loading on the thermal stability, flame retardant, anti-corrosive and mechanical properties of polyurethane nanocomposite for surface coating, Prog. Org. Coat. 89 (2015) 212–219.

[55] S. Han, X. Zhu, F. Chen, S. Chen, H. Liu, Flame-retardant system for rigid polyurethane foams based on diethyl bis (2-hydroxyethyl) aminomethylphosphonate and in-situ exfoliated clay, Polym. Degrad. Stab. 177 (2020), 109178.

[56] R. Lujan-Acosta, S. Sánchez-Valdes, E. Ramírez-Vargas, L.F. Ramos-DeValle, A. B. Espinoza-Martinez, O.S. Rodriguez-Fernandez, T. Lozano-Ramirez, P.G. Lafleur, Effect of amino alcohol functionalized polyethylene as compatibilizer for LDPE/EVA/clay/flame-retardant nanocomposites, Mater. Chem. Phys. 146 (2014) 437–445.

[57] Q. Zhang, D. Zhang, H. Xu, W. Lu, X. Ren, H. Cai, H. Lei, E. Huo, Y. Zhao, M. Qian, Biochar filled high-density polyethylene composites with excellent properties: towards maximizing the utilization of agricultural wastes, Ind. Crop. Prod. 146 (2020), 112185.

[58] Y. Guo, C.-C. Chang, G. Halada, M.A. Cuiffo, Y. Xue, X. Zuo, S. Pack, L. Zhang, S. He, E. Weil, Engineering flame retardant biodegradable polymer nanocomposites and their application in 3D printing, Polym. Degrad. Stab. 137 (2017) 205–215.

[59] A. Kausar, Flame retardant potential of clay nanoparticles, in: Clay Nanoparticles, Elsevier, 2020, pp. 169–184.

[60] S. Xiao, X. Hu, L. Jiang, Y. Ma, Y. Che, S. Zu, X. Jiang, Nano-ag modified bio-based loofah foam/polyethylene glycol composite phase change materials with higher photo-thermal conversion efficiency and thermal conductivity, J. Energy Storage 54 (2022), 105238.

[61] Y. Li, B. Wang, W. Zhang, J. Zhao, X. Fang, J. Sun, R. Xia, H. Guo, Y. Liu, Processing wood into a phase change material with high solar-thermal conversion efficiency

by introducing stable polyethylene glycol-based energy storage polymer, Energy 254 (2022), 124206.

[62] K. Yu, Y. Liu, Y. Yang, Enhanced thermal properties of polyethylene glycol/modified rice husk ash eco-friendly form-stable phase change material via optimizing support pore structure, J. Energy Storage 43 (2021), 103172.

[63] Z. Liu, K. Wei, S. Wang, B. Ma, X. Wang, W. Shi, J. Xu, Effect of high-temperature-resistant epoxy resin/polyethylene glycol 2000 composite stereotyped phase change material particles on asphalt properties, Constr. Build. Mater. 300 (2021), 124007.

[64] M.R. Yazdani, R. Ajdary, A. Kankkunen, O.J. Rojas, A. Seppälä, Cellulose nanofibrils endow phase-change polyethylene glycol with form control and solid-to-gel transition for thermal energy storage, ACS Appl. Mater. Interfaces 13 (2021) 6188–6200.

[65] C. Cheng, G. Cheng, F. Gong, Y. Fu, J. Qiao, Performance evaluation of asphalt mixture using polyethylene glycol polyacrylamide graft copolymer as solid–solid phase change materials, Constr. Build. Mater. 300 (2021), 124221.

[66] Y. Kobayashi, T. Saito, A. Isogai, Aerogels with 3D ordered nanofiber skeletons of liquid-crystalline nanocellulose derivatives as tough and transparent insulators, Angew.Chem. 126 (2014) 10562–10565.

[67] V. Apostolopoulou-Kalkavoura, K. Gordeyeva, N. Lavoine, L. Bergström, Thermal conductivity of hygroscopic foams based on cellulose nanofibrils and a nonionic polyoxamer, Cellulose 25 (2018) 1117–1126.